

## Article

# Modeling and Performance Optimization of an Irreversible Two-Stage Combined Thermal Brownian Heat Engine

Congzheng Qi<sup>1,2,3</sup>, Zemin Ding<sup>3</sup>, Lingen Chen<sup>1,2,\*</sup> , Yanlin Ge<sup>1,2</sup> and Huijun Feng<sup>1,2</sup>

<sup>1</sup> Institute of Thermal Science and Power Engineering, Wuhan Institute of Technology, Wuhan 430205, China; 18571499210@139.com (C.Q.); geyali9@hotmail.com (Y.G.); huijunfeng@139.com (H.F.)

<sup>2</sup> School of Mechanical & Electrical Engineering, Wuhan Institute of Technology, Wuhan 430205, China

<sup>3</sup> College of Power Engineering, Naval University of Engineering, Wuhan 430033, China; zeminding@hotmail.com

\* Correspondence: lgchenna@yahoo.com or lingenchen@hotmail.com

**Abstract:** Based on finite time thermodynamics, an irreversible combined thermal Brownian heat engine model is established in this paper. The model consists of two thermal Brownian heat engines which are operating in tandem with thermal contact with three heat reservoirs. The rates of heat transfer are finite between the heat engine and the reservoir. Considering the heat leakage and the losses caused by kinetic energy change of particles, the formulas of steady current, power output and efficiency are derived. The power output and efficiency of combined heat engine are smaller than that of single heat engine operating between reservoirs with same temperatures. When the potential field is free from external load, the effects of asymmetry of the potential, barrier height and heat leakage on the performance of the combined heat engine are analyzed. When the potential field is free from external load, the effects of basic design parameters on the performance of the combined heat engine are analyzed. The optimal power and efficiency are obtained by optimizing the barrier heights of two heat engines. The optimal working regions are obtained. There is optimal temperature ratio which maximize the overall power output or efficiency. When the potential field is subjected to external load, effect of external load is analyzed. The steady current decreases versus external load; the power output and efficiency are monotonically increasing versus external load.

**Keywords:** finite time thermodynamics; thermal Brownian heat engine; combined cycle; power output; efficiency; performance optimization



**Citation:** Qi, C.; Ding, Z.; Chen, L.; Ge, Y.; Feng, H. Modeling and Performance Optimization of an Irreversible Two-Stage Combined Thermal Brownian Heat Engine. *Entropy* **2021**, *23*, 419. <https://doi.org/10.3390/e23040419>

Academic Editor: Jean-Noël Jaubert

Received: 10 March 2021

Accepted: 29 March 2021

Published: 31 March 2021

**Publisher's Note:** MDPI stays neutral with regard to jurisdictional claims in published maps and institutional affiliations.



**Copyright:** © 2021 by the authors. Licensee MDPI, Basel, Switzerland. This article is an open access article distributed under the terms and conditions of the Creative Commons Attribution (CC BY) license (<https://creativecommons.org/licenses/by/4.0/>).

## 1. Introduction

Similar to macro motor, micro energy conversion devices can transfer energy in micro field, such as Brownian motor and energy selective electron engine. Brownian motor is a micro-nano device that can use micro-scale energy [1,2]. It realizes energy conversion through the movement of microscopic particles in viscous medium (VM) with different reservoirs. Many scholars studied the thermodynamic performance of such micro-motors and drew a lot of meaningful conclusions [3].

Finite time thermodynamics (FTT) theory [4–7] can consider various losses in actual processes and cycles and obtain more accurate results. In the studies of finite time thermodynamics, there exist two kinds of pivotal problems. The first one is to search the extreme of the optimization objective for a given cycle. Another one is to search the optimal path for a preset objective. FTT theory has been applied for performance optimization of various macro energy systems. The applications of FTT include many aspects and the two major aspects are optimal configurations [8–24] and optimal performances [25–68] studies.

Although the operating principles of micro-nano motors are quite different from those of macro motors, FTT theory is also applicable to the study of micro motors [1]. Thermal Brownian motor is driven by temperature difference. The particles migrate directionally and exchange energy with reservoirs. Research shows that the Brownian motor can work

as a heat engine (HE) or refrigerator. Asfaw and Bekele [69] modeled a thermal Brownian heat engine (TBHE) of a particle drifting in potential field. The heat flow expressions of the system were given. They proved that it could also work as refrigerator. Asfaw and Bekele [70] modeled a Brownian motor of a particle motioning in one-dimensional lattice. The regions of the system as HE or refrigerator were determined. Asfaw and Bekele [71] established a Brownian motor model. They obtained the parameters range of the system working as HE or refrigerator. Van den Broeck and Kawai [72] studied a completely solvable Brownian refrigerator model. The heat flow of the numerical calculation was compared with the result of the molecular dynamics simulation. Similarly, the Brownian motor can work as a heat pump. Ding et al. [73] modeled an irreversible thermal Brownian heat pump. The effects of parameters on system were analyzed. The range of basic parameters were obtained. Van den Broek et al. [74] analyzed a chiral Brownian heat pump model. The above scholars studied the performance of Brownian motor under three conditions.

Some scholars noticed that some irreversible losses cannot be ignored. Zhang et al. [75] studied a TBHE with kinetic energy loss. The curves of power and efficiency were loop-shaped. Zhang et al. [76] studied a TBHE model considered kinetic and potential energy loss under external load. They obtained the parameters of the system at maximum power or efficiency. Ai et al. [77,78] analyzed the irreversible TBHE [79] and refrigerator [80] with kinetic energy loss. The optimal characteristics of efficiency and coefficient of performance were obtained. Asfaw [81] researched the effect of serrated potential on TBHE. He found that the thermodynamic performance could be improved by subdividing the sawtooth potential. Asfaw [79] analyzed the effect of thermal inhomogeneity of potential field on TBHE. Some scholars studied Brownian motor by other methods. Gao et al. [80] analyzed the effect of irreversible losses on Onsager coefficients. Gao and Chen [82] established an equivalent TBHE model. They studied it with non-equilibrium thermodynamics theory and obtained the Onsager coefficients at maximum power. The research mentioned above mainly focused on the Brownian motors with two reservoirs. Different optimization objective functions, from power, efficiency to ecological function in single-stage Brownian motor have been studied widely [75,83–106]. The system models have been gradually improved and more universal results have been obtained.

For the one-stage HE, the heat in the cold reservoir (CR) is released into the environment directly and results in heat losses. To improve energy utilization efficiency, some scholars try to utilize waste heat by connecting the HEs by using FTT theory. For macro energy systems, Rubin and Andresen [107] modeled a three reservoirs endoreversible combined Carnot HE engine model with one as intermediate heat reservoir. Wu [108] optimized power of combined Carnot HE without intermediate heat reservoir. Chen [109] introduced the irreversibility factor to combined Carnot HE model. Ghasemkhani et al. [65] performed multiobjective optimization of combined Carnot HE. Some scholars [110–118] have also studied performance characteristics of combined Carnot HEs with various loss issues and different optimization objectives. For quantum energy systems, Meng et al. [119] modeled a three reservoirs endoreversible combined quantum Carnot HE with one as intermediate heat reservoir and Chen et al. [120] modeled irreversible two-stage combined HE with quantum gases.

## 2. Modeling of Irreversible Combined Thermal Brownian Heat Engine

Figure 1 shows an irreversible combined TBHE model working with three reservoirs with the temperatures  $T_H$ ,  $T_C$  and  $T_L$ . The model consists of two irreversibly TBHEs with different barrier height and the two TBHEs are operating in tandem. The bottom TBHE takes the CR of the topping TBHE as hot reservoir (HR). The lower TBHE absorbs heat from the CR of the upper TBHE. The heat dissipated by the upper TBHE is reused by lower TBHE. The intermediate reservoir  $T_C$  is the CR of the topping TBHE and the HR of the bottom TBHE.  $T_H$  is the HR of the topping TBHE and  $T_L$  is the CR of the bottom TBHE. There are thermal resistances between reservoir and VM and heat transfer rate is finite. The

operating temperatures of the topping TBHE are  $T_1$  and  $T_2$  and those for the bottom TBHE are  $T_3$  and  $T_4$ .

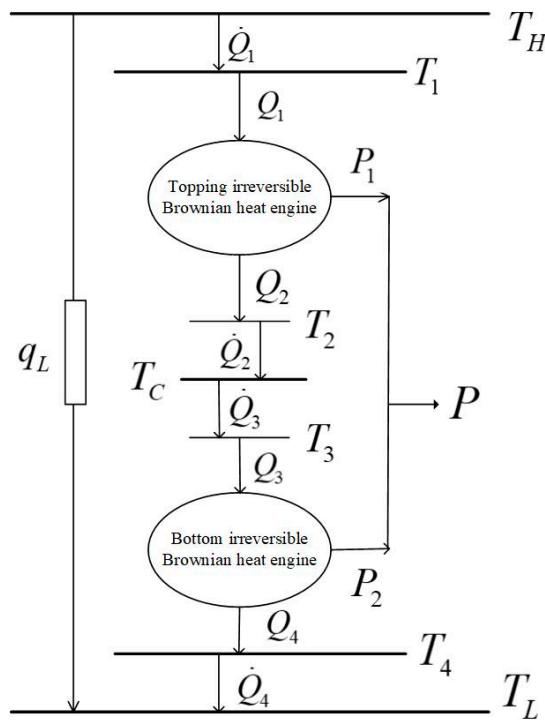


Figure 1. Irreversible combined thermal Brownian heat engine model.

The combined TBHE model without an intermediate HR is also feasible in theory. When the intermediate HR is not considered, the topping and bottom TBHEs transfer heat directly through viscous medium. As a result, the temperature of CR  $T_2$  of the topping HE and the HR  $T_3$  of the bottom HE is dynamic and the corresponding mathematical solution process becomes very complicated. Therefore, this paper introduces an intermediate reservoir to couple the topping and bottom HEs for determining the temperatures  $T_2$  and  $T_3$ , similar to that in Ref. [107], for macro combined HE, with which the subsequent solution process is greatly simplified.

The method used in this paper can also be used to research the combined TBHE model without the intermediate HR. Similar research work has been performed for macroscopic combined Carnot HE models without the intermediate HR [108,109]. The performance analysis and optimization of combined TBHE without the intermediate HR will be carried out in future work.

Figure 2 is the schematic diagram of the combined TBHE. The particle moves in VM with period sawtooth potential field and exchanges heat with the reservoirs through the VM. The VM is an essential part of the present TBHE model without which the Brownian motor cannot move and the entire system cannot operate normally. The potential is electric potential field with different energy heights at different positions. When two TBHEs are operating stably, the model works as a combined TBHE. The model of the micro combined TBHE which can realize multi-stage utilization of energy is established. This research provides a new idea to realize microscopic energy utilization at thermal Brownian motor.

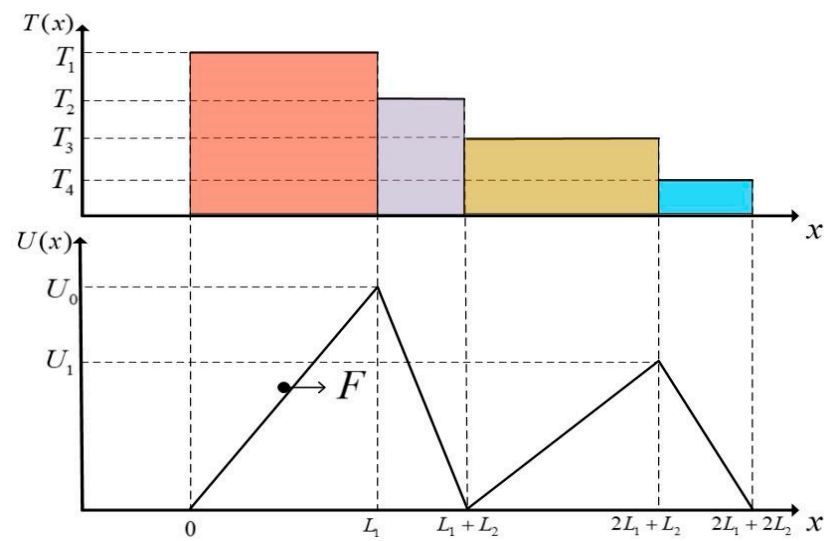


Figure 2. Schematic diagram of combined TBHE.

For the topping TBHE, the heat absorption rate is  $Q_1$ ; the heat releasing rate is  $Q_2$ ; and the power output is  $P_1$ . For the bottom TBHE, the heat absorption rate is  $Q_3$ ; the heat releasing rate is  $Q_4$ ; and the power output is  $P_2$ . For the combined TBHE, the total power output is  $P$ .  $q_L$  is bypass heat leakage rate between  $T_H$  and  $T_L$ . It is supposed that the thermal conductivities between the reservoir and the VM are all constant and the temperatures of the reservoirs and VM will not change with time when the system is operating stably. Therefore,  $T_H > T_1 > T_2 > T_C > T_3 > T_4 > T_L$  holds.

The temperature of VM  $T(x)$  and the sawtooth potential  $U(x)$  are, respectively:

$$T(x) = \begin{cases} T_1, & 0 < x \leq L_1 \\ T_2, & L_1 < x \leq L_1 + L_2 \\ T_3, & L_1 + L_2 < x \leq 2L_1 + L_2 \\ T_4, & 2L_1 + L_2 < x \leq 2(L_1 + L_2) \end{cases} \quad (1)$$

$$U(x) = \begin{cases} U_0 x / L_1, & 0 < x \leq L_1 \\ U_0(L_1 / L_2 - x / L_2 + 1), & L_1 < x \leq L_1 + L_2 \\ U_1(x / L_1 - L_2 / L_1 - 1), & L_1 + L_2 < x \leq 2L_1 + L_2 \\ U_1(-x / L_2 + 2L_1 / L_2 + 2), & 2L_1 + L_2 < x \leq 2L_1 + 2L_2 \end{cases} \quad (2)$$

where  $L_1$  and  $L_2$  are the lengths of potential field;  $U_0$  and  $U_1$  are barrier heights of potential field and the total cycle length is  $2L(L = L_1 + L_2)$ . The sawtooth potential field represents a class of actions which is linearly related to the external load. The barrier height of the potential field is different under different operation conditions. Through the application of a linear sawtooth potential, the mathematical analysis process of the TBHE with inhomogeneous VM can be effectively simplified. Asfaw and Bekele [69] firstly simplified the process of solving the dynamic equation greatly by introducing a sawtooth potential field for the TBHE. The analytical results of Smoluchowski equation make it possible to study the analytical model of a TBHE [69]. In addition, other different kinds of potential fields can be also applied into the study of the TBHE model. Asfaw [81] studied the TBHE with periodic rugged potential field. Asfaw and Bekele [70] and Asfaw [91] studied the TBHE models with discrete ratchet potential. Cheng et al. [121] studied the TBHE with periodic double-barrier sawtooth potential field. This paper studies the TBHE with linear potential field on the bases of previous studies. The application of nonlinear potential field in combined TBHE model will be considered in future research.

When the system works stably, the particle will drift in a directional manner. The heat caused by the friction of Brownian particles through the VM can be expressed as  $\gamma vL$ , and  $\gamma v$  is friction. The average drift velocity of the particle in a cycle length  $L$  ( $v = JL$ )

is  $v$ , and  $J$  is the drift velocity of the particle at position  $z$  ( $0 < z < L$ ). The expression of  $J$  is very complicated; therefore, the self-defined parameters such as  $G$ ,  $H$  and  $I$  are introduced to simplify the analytical expression of  $J$ . Because of the different barrier heights and operating temperatures of two TBHEs, the steady current is different. The steady current  $J$  of upper or lower HE is closely related to the variables such as barrier height  $U$ , external load  $F$ , the length of potential field  $L$ , temperature  $T$ , the position of particle  $z$  and time  $t$ . The analytical expression of  $J$  is solved from the Smoluchowski equation for the Brownian particle under specific position  $z$  and time  $t$ , which makes it possible to analyze the performance of the Brownian motor with a solvable model. According to Refs. [70,75], the steady currents  $J_1$  and  $J_2$  of topping and bottom TBHEs are

$$J_1 = -I_1 / (G_1 G_2 + H_1 I_1) \quad (3)$$

$$J_2 = -I_2 / (G_3 G_4 + H_2 I_2) \quad (4)$$

where the self-defined functions  $I_1$ ,  $I_2$ ,  $H_1$ ,  $H_2$ ,  $G_1$ ,  $G_2$ ,  $G_3$  and  $G_4$  are, respectively given by:

$$I_1 = e^{a-b} - 1, I_2 = e^{c-d} - 1 \quad (5)$$

$$H_1 = A_1 + B_1 + C_1, H_2 = A_2 + B_2 + C_2 \quad (6)$$

$$G_1 = (L_1/aT_1)(1 - e^{-a}) + (e^{-a}L_2/bT_2)(e^b - 1), G_2 = (\gamma L_1/a)(e^a - 1) + (\gamma e^a L_2/b)(1 - e^{-b}) \quad (7)$$

$$G_3 = (L_1/cT_3)(1 - e^{-c}) + (e^{-c}L_2/bT_4)(e^d - 1), G_4 = (\gamma L_1/c)(e^c - 1) + (\gamma e^c L_2/d)(1 - e^{-d}) \quad (8)$$

where  $\gamma$  is the friction coefficient of particles and the self-defined functions  $A_1$ ,  $B_1$ ,  $C_1$ ,  $A_2$ ,  $B_2$  and  $C_2$  are, respectively:

$$A_1 = (\gamma L_1^2/a^2 T_1)(e^{-a} + a - 1), B_1 = (\gamma L_1 L_2/ab T_2)(1 - e^{-a})(e^b - 1), C_1 = (\gamma L_2^2/b^2 T_2)(e^b - b - 1) \quad (9)$$

$$A_2 = (\gamma L_1^2/c^2 T_3)(e^{-c} + c - 1), B_2 = (\gamma L_1 L_2/cd T_4)(1 - e^{-c})(e^d - 1), C_2 = (\gamma L_2^2/d^2 T_4)(e^d - d - 1) \quad (10)$$

$$a = (U_0 + FL_1)/T_1, b = (U_0 - FL_2)/T_2 \quad (11)$$

$$c = (U_1 + FL_1)/T_3, d = (U_1 - FL_2)/T_4 \quad (12)$$

where  $F$  is external load. The drift velocity  $v$  of particles is  $v = JL$ .

There are three kinds of heat flows for the TBHE. The first is the heat transfer rate when a particle passes through the potential field. The particle absorbs energy to overcome external load  $F$  and viscous forces  $\gamma v$ . The heat absorption and releasing rates of the topping and bottom TBHEs can be expressed as

$$Q_1 = U_0 + (F + \gamma v_1)L_1 \quad (13)$$

$$Q_2 = U_0 - (F + \gamma v_1)L_2 \quad (14)$$

$$Q_3 = U_1 + (F + \gamma v_2)L_1 \quad (15)$$

$$Q_4 = U_1 - (F + \gamma v_2)L_2 \quad (16)$$

The second is the energy due to kinetic energy change when a particle moves. The heat flows can be expressed as [122,123]

$$q_{kin1} = k_B(T_1 - T_2)/2 \quad (17)$$

$$q_{kin2} = k_B(T_3 - T_4)/2 \quad (18)$$

where  $k_B$  is Boltzmann constant,  $q_{kin1}$  and  $q_{kin2}$  are the energy losses of topping and bottom TBHEs, respectively.

The third is the bypass heat leakage rate  $q_L$  between reservoirs, which can be expressed as [124–126].

$$q_L = C_i(T_H - T_L) \quad (19)$$

where  $C_i$  is heat leakage coefficient.

### 3. Main Performance Parameters

According to Equations (13)–(19), the total heat absorption rate  $\dot{Q}_1$  and releasing rate  $\dot{Q}_2$  of the topping TBHE are

$$\dot{Q}_1 = Q_1 + q_{kin1} + q_L = U_0 + (F + \gamma v_1)L_1 + k_B(T_1 - T_2)/2 + C_i(T_H - T_L) \quad (20)$$

$$\dot{Q}_2 = Q_2 + q_{kin1} = U_0 - (F + \gamma v_1)L_2 + k_B(T_1 - T_2)/2 \quad (21)$$

The power output  $P_1$  is

$$P_1 = \dot{Q}_1 - \dot{Q}_2 = (F + \gamma v_1)L + C_i(T_H - T_L) \quad (22)$$

The total heat absorption rate  $\dot{Q}_3$  and releasing rate  $\dot{Q}_4$  of the bottom TBHE are

$$\dot{Q}_3 = Q_3 + q_{kin2} = U_1 + (F + \gamma v_2)L_1 + k_B(T_3 - T_4)/2 \quad (23)$$

$$\dot{Q}_4 = Q_4 + q_{kin2} + q_L = U_1 - (F + \gamma v_2)L_2 + k_B(T_3 - T_4)/2 + C_i(T_H - T_L) \quad (24)$$

The power output  $P_2$  is

$$P_2 = \dot{Q}_3 - \dot{Q}_4 = (F + \gamma v_2)L - C_i(T_H - T_L) \quad (25)$$

The total  $P$  and  $\eta$  of the combined TBHE are

$$P = P_1 + P_2 = (F + \gamma v_1)L + (F + \gamma v_2)L \quad (26)$$

$$\eta = \frac{P}{\dot{Q}_1} = \frac{(F + \gamma v_1)L + (F + \gamma v_2)L}{U_0 + (F + \gamma v_1)L_1 + k_B(T_1 - T_2)/2 + C_i(T_H - T_L)} \quad (27)$$

In order to simplify calculation, some dimensionless parameters are defined: the asymmetry of the potential  $\mu = L_1/L$ , the dimensionless barrier height  $U = U_0/(k_B T_H)$ , the ratio of barrier height  $n = U_0/U_1$ , the dimensionless external load  $f = FL/(k_B T_H)$ ,  $\beta = C_i/k_B$ ,  $\tau = T_L/T_H$ ,  $\omega = T_C/T_H$ ,  $k_1 = T_L/T_4$ ,  $k_2 = T_3/T_C$ ,  $k_3 = T_C/T_2$  and  $k_4 = T_1/T_H$ . It is future defined that  $a = k_B(U + \mu f)/k_4$ ,  $b = k_3 k_B[U - (1 - \mu)f]/\omega$ ,  $c = k_B(U/n + \mu f)/k_2 \omega$  and  $d = k_1 k_B[U/n - (1 - \mu)f]/\tau$ . The dimensionless forms of  $J_1$ ,  $J_2$ ,  $P$  and the efficiency  $\eta^*$  can be rewritten as follows:

$$J_1^* = \frac{J_1 \gamma L^2}{k_B T_H} = \frac{(1 - e^{a-b})/k_B}{x_0 + (e^{a-b} - 1)y_0} \quad (28)$$

$$J_2^* = \frac{J_2 \gamma L^2}{k_B T_H} = \frac{(1 - e^{c-d})/k_B}{x_1 + (e^{c-d} - 1)y_1} \quad (29)$$

$$P^* = \frac{P}{k_B T_H} = 2f + \frac{(1 - e^{a-b})/k_B}{x_0 + (e^{a-b} - 1)y_0} + \frac{(1 - e^{c-d})/k_B}{x_1 + (e^{c-d} - 1)y_1} \quad (30)$$

$$\eta^* = \eta = \frac{2f + [(1 - e^{a-b})/k_B]/[x_0 + (e^{a-b} - 1)y_0] + [(1 - e^{c-d})/k_B]/[x_1 + (e^{c-d} - 1)y_1]}{U + \mu f + [\mu(1 - e^{a-b})/k_B]/[x_0 + (e^{a-b} - 1)y_0] + (k_4 - \omega/k_3)/2 + \beta(1 - \tau)} \quad (31)$$

The self-defined functions  $x_0, y_0, x_1$  and  $y_1$  are introduced to simplify the writing processes. These functions are defined as, respectively:

$$x_0 = \left[ \frac{\mu(1 - e^{-a})}{ak_4} + \frac{k_3e^{-a}(1 - \mu)(e^b - 1)}{b\omega} \right] \left[ \frac{\mu(e^a - 1)}{a} + \frac{e^a(1 - \mu)(1 - e^{-b})}{b} \right] \tag{32}$$

$$y_0 = \frac{\mu^2(e^{-a} + a - 1)}{a^2k_4} + \frac{\mu k_3(1 - \mu)(1 - e^{-a})(e^b - 1)}{ab\omega} + \frac{k_3(1 - \mu)^2(e^b - b - 1)}{b^2\omega} \tag{33}$$

$$x_1 = \left[ \frac{\mu(1 - e^{-c})}{ck_2\omega} + \frac{k_1e^{-c}(1 - \mu)(e^d - 1)}{d\tau} \right] \left[ \frac{\mu(e^c - 1)}{c} + \frac{e^c(1 - \mu)(1 - e^{-d})}{d} \right] \tag{34}$$

$$y_1 = \frac{\mu^2(e^{-c} + c - 1)}{c^2k_2\omega} + \frac{\mu(1 - \mu)k_1(1 - e^{-c})(e^d - 1)}{cd\tau} + \frac{k_1(1 - \mu)^2(e^d - d - 1)}{d^2\tau} \tag{35}$$

#### 4. Optimal Performance Characteristics without External Load

##### 4.1. Performance Analysis without External Load

When the combined TBHE is free from external load ( $f = 0$ ), the analytical expressions of power ( $P^*$ ) and efficiency ( $\eta^*$ ) are

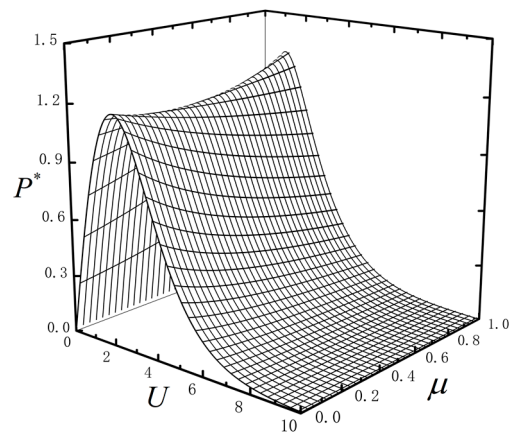
$$P^* = \frac{Pt}{k_B T_H} = \frac{(1 - e^{a-b})t/k_B}{x_0 + (e^{a-b} - 1)y_0} + \frac{(1 - e^{c-d})t/k_B}{x_1 + (e^{c-d} - 1)y_1} \tag{36}$$

$$\eta^* = \frac{[(1 - e^{a-b})/k_B]/[x_0 + (e^{a-b} - 1)y_0] + [(1 - e^{c-d})/k_B]/[x_1 + (e^{c-d} - 1)y_1]}{U + [\mu(1 - e^{a-b})/k_B]/[x_0 + (e^{a-b} - 1)y_0] + (k_4 - \omega/k_3)/2 + \beta(1 - \tau)} \tag{37}$$

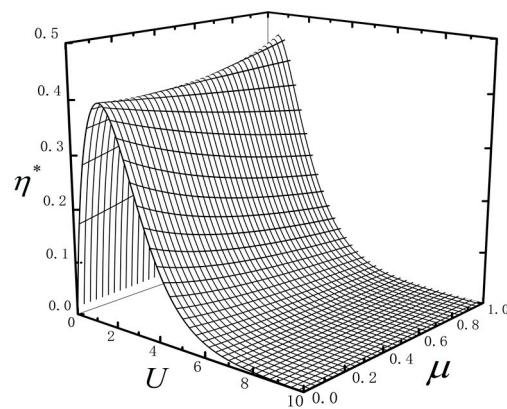
where  $a = k_B U/k_4, b = k_3 k_B U/\omega, c = k_B U/nk_2\omega$  and  $d = k_1 k_B U/n\tau$ .

The performance parameters  $P^*$  and  $\eta^*$  are the functions of variables such as  $U, n, \mu, k_i (i = 1, 2, 3, 4), \omega$  and  $\tau$ . When the temperature of reservoirs  $T_H$  and  $T_L$  are fixed, the temperature ratio  $\tau = T_L/T_H$  is fixed. The temperature of intermediate reservoir is  $T_C$ . The parameter  $\omega (\omega = T_C/T_H)$  is defined as the temperature ratio of intermediate reservoir to the HR. Due to  $T_L < T_C < T_H$ , one has  $0 < \tau < \omega < 1$ . The dimensionless barrier height  $U (U = U_0/(k_B T_H))$  is taken as a major control variable of the system. The ratio of barrier height is defined as  $n = U_0/U_1$  and one has  $n > 0$ . The asymmetry of the potential is defined as  $\mu = L_1/L$  and one has  $0 < \mu < 1$ . These variables will affect the performance directly. Therefore, it is necessary to analyze their effects emphatically. The performance of the combined TBHE without external load is analyzed by numerical calculation. To simplify the analyses, it is supposed that the thermal conductivities are equal between reservoir and vicious medium and  $k = k_1 = k_2 = k_3 = k_4$ . The combined TBHE is operating between reservoirs with fixed temperature  $T_H$  and  $T_L$ , and  $\tau$  is fixed.

Figure 3 shows  $P^*$  and  $\eta^*$  characteristics about  $U$  and  $\mu$  with  $\tau = 0.1, \omega = 0.4, k = 0.95, n = 2$  and  $C_i = 2$ . The  $P^*$  and  $\eta^*$  performance characteristics are similar. When  $\mu$  is fixed,  $P^*$  and  $\eta^*$  have maximums about  $U$ . This is because the barrier height affects the motion and the heat exchange of particle. The steady current increases with the increase of barrier height and the  $P^*$  and  $\eta^*$  increase; as the barrier height gets higher and higher, the steady current decreases but the absorbed rate increases from HR  $T_H$  and the  $P^*$  and  $\eta^*$  decrease. when  $U$  is fixed,  $P^*$  and  $\eta^*$  are monotonous about  $\mu$ . The maximum power ( $P_{max}^*$ ) and maximum efficiency ( $\eta_{max}^*$ ) decrease first and then increase versus  $\mu$ . The heat absorption of the particle for overcoming friction is influenced by the parameter  $\mu$ .



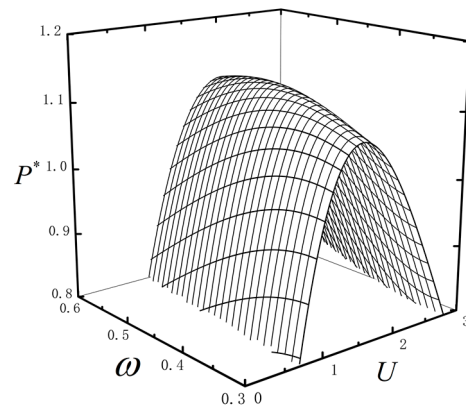
(a)  $P^*$  characteristic about  $U$  and  $\mu$ .



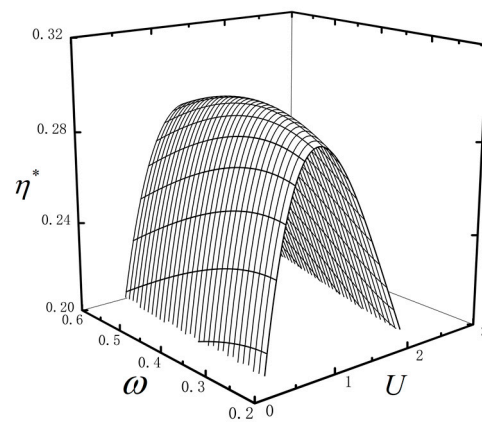
(b)  $\eta^*$  characteristic about  $U$  and  $\mu$ .

**Figure 3.**  $P^*$  and  $\eta^*$  characteristics about  $U$  and  $\mu$ .

Figure 4 show  $P^*$  and  $\eta^*$  characteristics about  $U$  and  $\omega$  with  $\tau = 0.1$ ,  $\mu = 0.4$ ,  $k = 0.95$ ,  $n = 2$  and  $C_i = 2$ . It is shown that the performance of the combined TBHE is closely related to the temperature ratio  $\omega$ . When  $\tau$  and  $U$  are fixed,  $P^*$  and  $\eta^*$  have peaks about  $\omega$ . That means that when  $T_H$  and  $T_L$  are fixed, there is an optimal temperature  $T_C$  for the intermediate reservoir to maximize  $P^*$  or  $\eta^*$ . Figures 3 and 4 research the characteristics of the  $P^*$  and  $\eta^*$  about  $\mu$  or  $\omega$  with different parameters. Although the shapes of the figures are similar, the values of the corresponding parameters are different when the power and efficiency are maximized. This section studies the performance characteristics of the system operating at maximum power or efficiency and explains the operating principle. Therefore, Figures 3 and 4 show the above shapes.



(a)  $P^*$  characteristic about  $U$  and  $\omega$ .



(b)  $\eta^*$  characteristic about  $U$  and  $\omega$ .

Figure 4.  $P^*$  and  $\eta^*$  characteristics about  $U$  and  $\omega$ .

Figure 5 shows the curves of  $P^*-\eta^*$  about  $C_i$ . The curve is parabolic one if  $q_L$  and  $q_{kin}$  are ignored as shown by curve 1; and it is loop-shaped one if  $q_L$  and  $q_{kin}$  are considered. The effects of heat leakage and the heat flow due to the change of kinetic energy on the system performance are similar to the effect of heat leakage on the macro thermodynamic systems. Therefore, the curve of power output and efficiency presents a loop-shaped characteristic similar to macro heat engine. When  $C_i$  increases, the area of the loop-shaped curve decreases; the power  $P^*_{max}$  remains constant whereas the efficiency  $\eta_{max}$  decreases. The optimal working regions are  $P^*_{\eta^*_{max}} < P^* < P^*_{max}$  and  $\eta^*_{P^*_{max}} < \eta^* < \eta^*_{max}$ , where both  $P^*$  and  $\eta^*$  can be maintained as large.

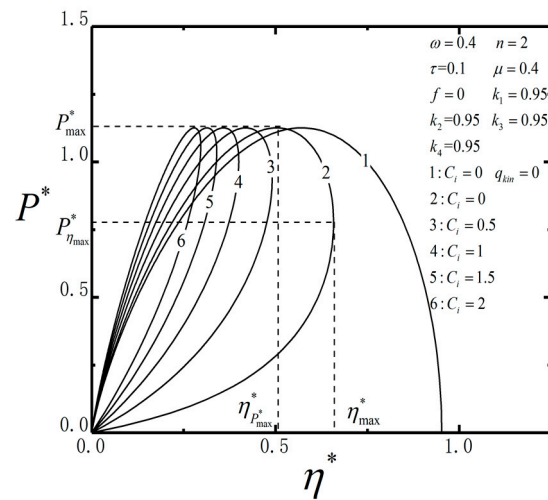
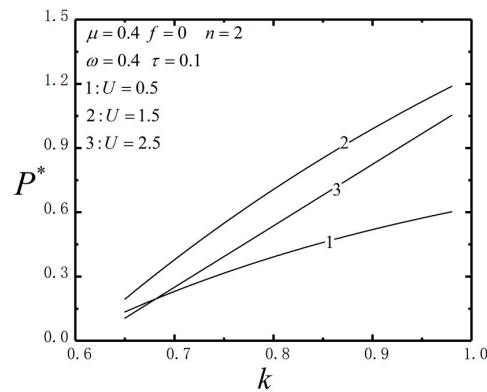
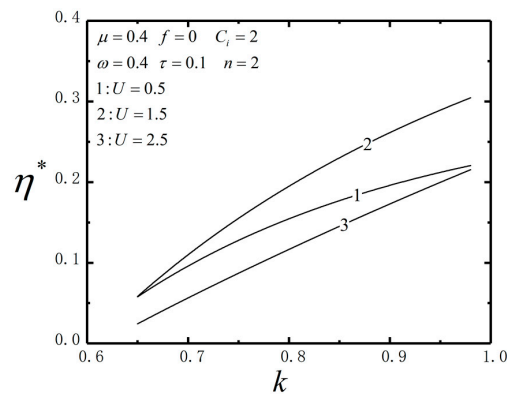


Figure 5. The curves of  $P^* - \eta^*$  about  $C_i$ .

Figure 6 shows the characteristics of  $P^*$  and  $\eta^*$  versus  $k$  with  $\tau = 0.1, \mu = 0.4, n = 2, \omega = 0.4$  and  $C_i = 2$ .  $P^*$  and  $\eta^*$  monotonically increase about  $k$ . It indicates that the higher the thermal conductivities between the vicious medium and reservoir, the better  $P^*$  and  $\eta^*$  of the combined TBHE. Enhancing the heat transfer between reservoir and TBHE can improve  $P^*$  and  $\eta^*$  of the system.



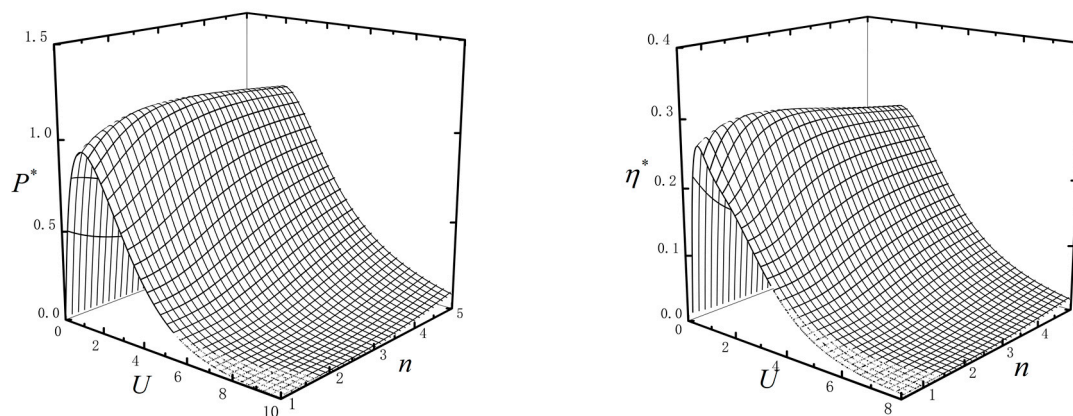
(a) The curves of  $P^*$  versus  $k$



(b) The curves of  $\eta^*$  versus  $k$

Figure 6.  $P^*$  and  $\eta^*$  characteristics versus  $k$ .

According to above analyses, one can find that the barrier height  $U$  has obvious impact on the system performance. When the upper heat engine works normally, the performance of lower heat engine can be optimized by adjusting the barrier height of the lower engine and the performance of the combined system can be optimized. Therefore, the relationship between barrier heights  $U_0$  and  $U_1$  of the two-stage combined TBHE is studied in detail. Figure 7 shows the  $P^*$  and  $\eta^*$  characteristics about  $U$  and  $n$  without external load with  $\tau = 0.1, C_i = 2, \omega = 0.4, \mu = 0.4$  and  $k = 0.95$ . It can be seen that  $P^*$  and  $\eta^*$  have peaks about  $U$  and  $n$ . There are appropriate  $U$  and  $n$  which maximize  $P^*$  or  $\eta^*$ , respectively. When the topping HE operating is stable, the barrier height of bottom HE can be adjusted to make the combined TBHE operating at optimal performance. It is of great significance for the analysis and parameter design of combined TBHE.



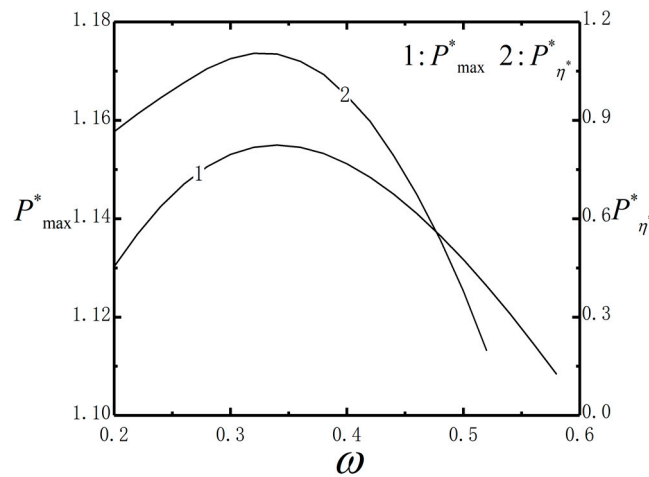
(a)  $P^*$  characteristic about  $U$  and  $n$  without  $f$ . (b)  $\eta^*$  characteristic about  $U$  and  $n$  without  $f$ .

Figure 7.  $P^*$  and  $\eta^*$  characteristics about  $U$  and  $n$  without  $f$ .

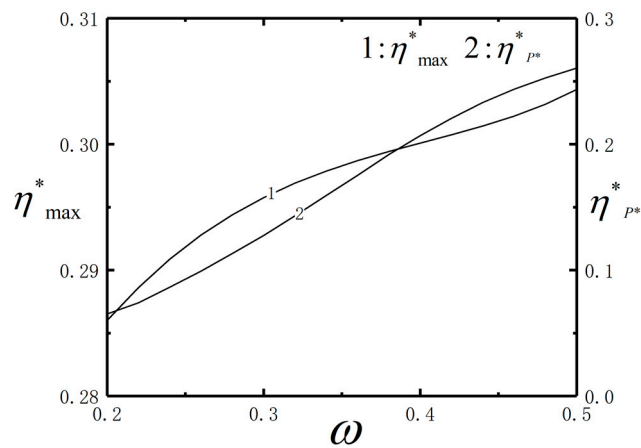
#### 4.2. Optimal Performance without External Load

When  $(\partial P^* / \partial U)_n = 0$  and  $(\partial P^* / \partial n)_U = 0$ , according to Equations (36) and (37),  $P^*_{\max}$  and the corresponding efficiency ( $\eta^*_{P^*}$ ) can be obtained. Similarly, when  $\eta^*$  is maximized,  $\eta^*_{\max}$  and the corresponding power ( $P^*_{\eta^*}$ ) can be obtained by the method of evaluation extreme value. The performance analysis and optimization work performed for the combined two-stage thermal Brownian heat engine belongs to the first type of research problem of finite time thermodynamics. Due to its special working mechanism, the expressions of performance parameters such as power and efficiency respect to its design parameters are highly non-linear. It is very difficult to obtain the analytical solution. Therefore, numerical methods are applied for intensive analyses.

Figure 8 shows the performance of dimensionless power output ( $P^*_{\max}, P^*_{\eta^*}$ ) and efficiency ( $\eta^*_{\max}, \eta^*_{P^*}$ ) versus  $\omega$  with the optimal barrier height. The variation ranges of  $P^*_{\max}$  and  $\eta^*_{\max}$  are small, but the variation ranges of  $P^*_{\eta^*}$  and  $\eta^*_{P^*}$  are large. After optimizing the barrier heights  $U_0$  and  $n$ ,  $\eta^*_{\max}$  is monotonically increasing versus  $\omega$ . This is different from the results shown by Figure 5, where the  $\eta^*_{\max}$  increases firstly, and then decreases. The  $P^*_{\max}$  and  $\eta^*_{\max}$  cannot be satisfied simultaneously. Different optimization objectives can be chosen under different design requirement.



(a) The curves of dimensionless power output under different objectives.



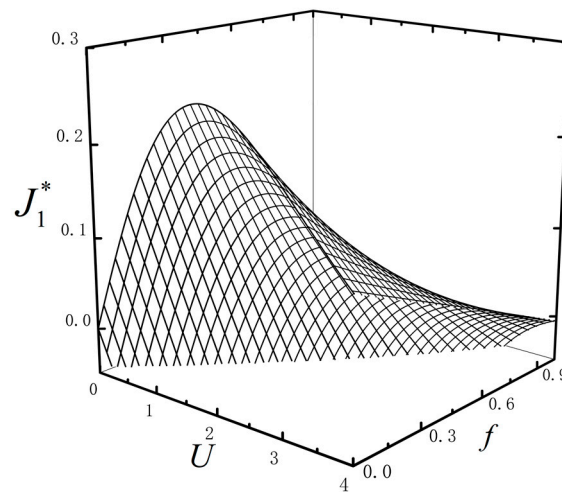
(b) The curves of efficiency under different objectives.

**Figure 8.** The curves of dimensionless power output and efficiency under different objectives.

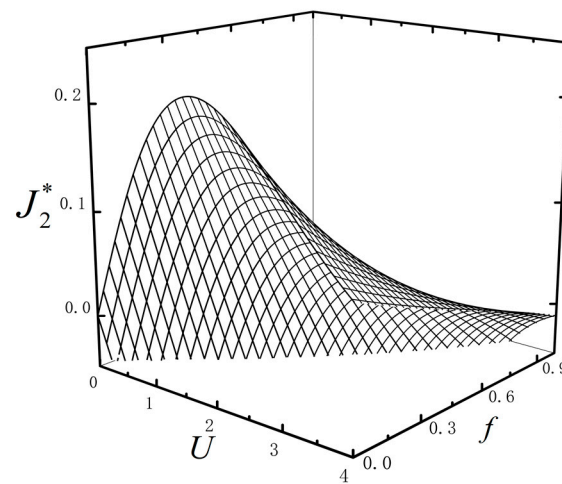
### 5. The Performance Characteristics with External Load

The barrier height will change when the potential field is influenced by external load, which will affect the movement of the particle. Therefore, the performance of the system needs to be further analyzed.

Figure 9 shows the characteristics  $J_1^*$  and  $J_2^*$  about  $U$  and  $f$  with  $\omega = 0.4$ ,  $\tau = 0.2$ ,  $\mu = 0.4$ ,  $k = 0.8$ ,  $n = 2$  and  $C_i = 2$ . The steady current decreases monotonically with external load. This indicates that the velocity of the particles decreases when the sawtooth potential is acted upon by external load. When external load  $f$  increases further,  $J_1^*$  or  $J_2^*$  is less than zero. This means that the particle moves in the opposite direction and the Brownian motor works as a refrigerator. If the combined TBHE works normally, the particles are moving to the right for the topping and bottom TBHEs. The external load  $f$  should satisfy  $J_1^* > 0$  and  $J_2^* > 0$ .



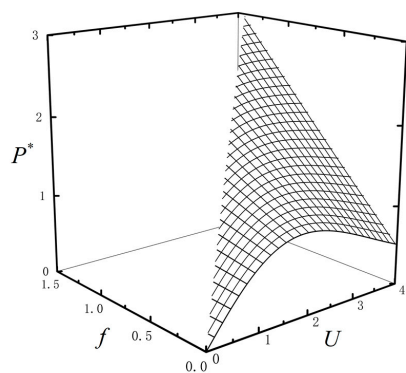
(a) The characteristic of  $J_1^*$  about  $U$  and  $f$ .



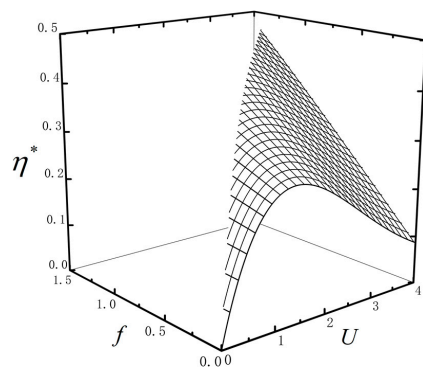
(b) The characteristic of  $J_2^*$  about  $U$  and  $f$ .

**Figure 9.** The characteristics of  $J_1^*$  and  $J_2^*$  about  $U$  and  $f$ .

Figure 10 shows the characteristics of  $P^*$  and  $\eta^*$  about  $U$  and  $f$  with  $\omega = 0.4$ ,  $\tau = 0.2$ ,  $\mu = 0.4$ ,  $k = 0.8$ ,  $n = 2$  and  $C_i = 2$ . Figure 11 shows the characteristics of  $P^*$  and  $\eta^*$  about  $f$  and  $\mu$  with  $\omega = 0.4$ ,  $\tau = 0.2$ ,  $U = 2$ ,  $k = 0.8$ ,  $n = 2$  and  $C_i = 2$ .  $P^*$  and  $\eta^*$  are monotonically increasing versus  $f$ . The reason is that the particle needs to absorb heat in order to overcome external load.  $P^*$  and  $\eta^*$  increase first and then decreasing versus  $U$  when  $f$  is small; but  $P^*$  and  $\eta^*$  are monotonically decreasing versus  $U$  when  $f$  is large. The surfaces are truncated as shown by Figure 10. This is because when the barrier height  $U_0$  and  $U_1$  are fixed, the external load  $f$  can't be too large if the combined TBHE is to work normally. When  $f$  is fixed,  $\mu$  has little impact on  $P^*$  and  $\eta^*$ . However,  $P_{\max}^*$  and  $\eta_{\max}^*$  are monotonically increasing versus  $\mu$  as shown by Figure 11. The heat absorption of the particle for overcoming external load is influenced by the parameter  $\mu$ .

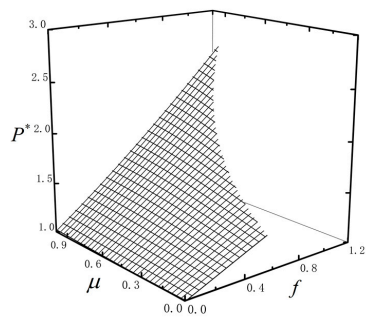


(a)  $P^*$  characteristic about  $U$  and  $f$ .

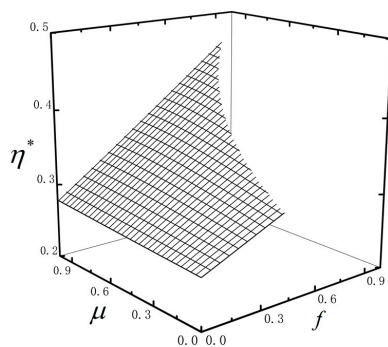


(b)  $\eta^*$  characteristic about  $U$  and  $f$ .

Figure 10.  $P^*$  and  $\eta^*$  characteristics about  $U$  and  $f$ .



(a)  $P^*$  characteristic about  $f$  and  $\mu$ .



(b)  $\eta^*$  characteristic about  $f$  and  $\mu$ .

Figure 11.  $P^*$  and  $\eta^*$  characteristics about  $f$  and  $\mu$ .

Figure 12 shows the characteristics of  $P^*$  and  $\eta^*$  versus  $n$  with different  $f$ . External load makes  $P^*$  and  $\eta^*$  increased significantly. When  $U$  is fixed, there is an optimal  $n_{P^*}$  (or  $n_{\eta^*}$ ) to maximize  $P^*$  (or  $\eta^*$ ). When the upper HE works normally, the performance of lower HE can be optimized by adjusting the barrier height of the lower engine and the performance of the combined TBHE can be improved. If the ratio of barrier height is set properly,  $P^*$  or  $\eta^*$  will increase. These characteristics are consistent with Figure 7.

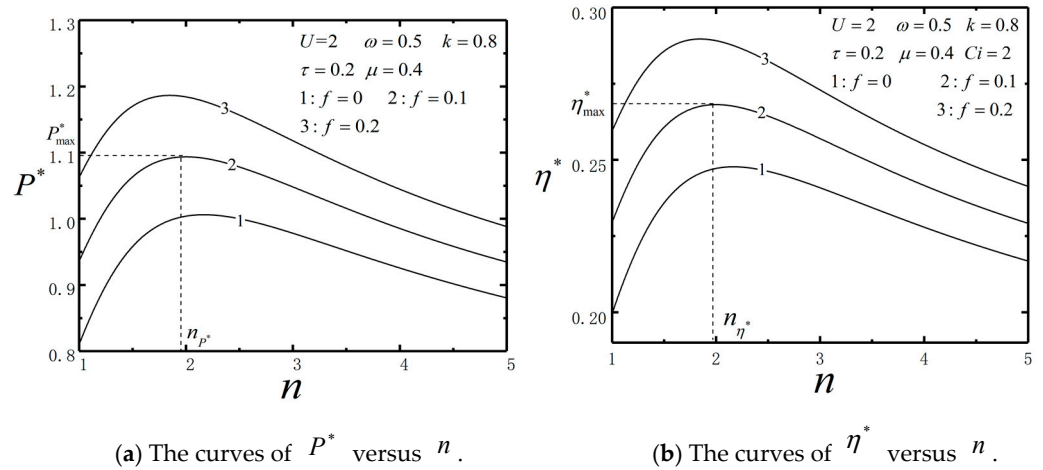


Figure 12.  $P^*$  and  $\eta^*$  characteristics versus  $n$ .

### 6. Performance Comparison with Single Cycle

The combined TBHE can improve power output and efficiency effectively by expanding the temperature range. In order to explore the differences between the micro and macro combined HEs, this section compares the performance characteristics with macro combined HE. For the irreversible single TBHE operating between reservoirs  $T_H$  and  $T_L$ , it is supposed that the temperatures of VM remains at  $T_1$  and  $T_4$ , the power output  $P_1^*$  and efficiency  $\eta_1^*$  are [75]:

$$P_3^* = f + \frac{(1 - e^{a_1 - b_1})/k_B}{x_2 + (e^{a_1 - b_1} - 1)y_2} \tag{38}$$

$$\eta_3^* = \frac{f + [(1 - e^{a_1 - b_1})/k_B]/[x_2 + (e^{a_1 - b_1} - 1)y_2]}{U + \mu f + [\mu(1 - e^{a_1 - b_1})/k_B]/[x_2 + (e^{a_1 - b_1} - 1)y_2] + (k_4 - \tau/k_1)/2 + \beta(1 - \tau)} \tag{39}$$

where the self-defined functions  $a_1, b_1, x_2$  and  $y_2$  are, respectively:

$$a_1 = k_B(U + \mu f)/k_4, \quad b_1 = k_1 k_B[U - (1 - \mu)f]/\tau \tag{40}$$

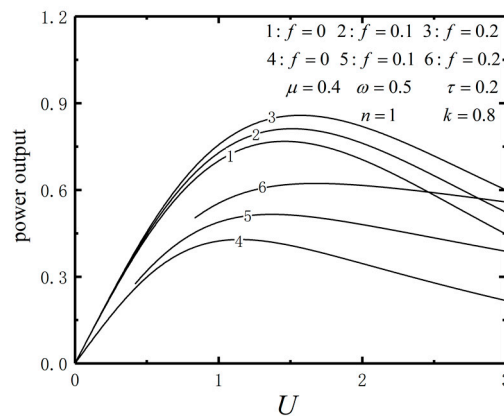
$$x_2 = \left[ \frac{\mu(1 - e^{-a_1})}{a_1 k_4} + \frac{k_1 e^{-a_1}(1 - \mu)(e^{b_1} - 1)}{b_1 \tau} \right] \left[ \frac{\mu(e^{a_1} - 1)}{a_1} + \frac{e^{a_1}(1 - \mu)(1 - e^{-b_1})}{b_1} \right] \tag{41}$$

$$y_2 = \frac{\mu^2(e^{-a_1} + a_1 - 1)}{a_1^2 k_4} + \frac{\mu k_1(1 - \mu)(1 - e^{-a_1})(e^{b_1} - 1)}{a_1 b_1 \tau} + \frac{k_1(1 - \mu)^2(e^{b_1} - b_1 - 1)}{b_1^2 \tau} \tag{42}$$

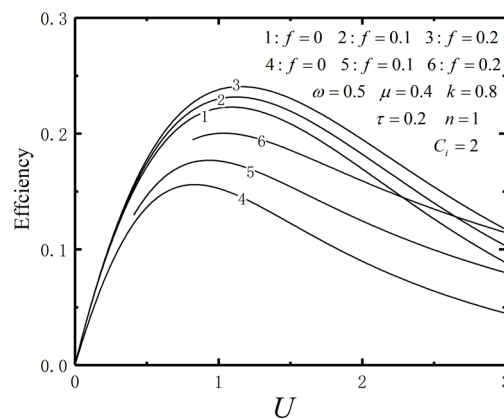
The performance comparison is illustrated by numerical calculation. The parameters are set as  $\omega = 0.5, \tau = 0.2, \mu = 0.4, k = 0.8, n = 1$  and  $C_i = 2$ . Figure 13 shows the  $P^*$  and  $\eta^*$  versus  $U$  curves of the irreversible single TBHE (curves 1–3) and irreversible combined TBHE (curves 4–6), respectively. Tables 1 and 2 list the power output and efficiency performance comparison between single and combined TBHE with  $U = 1.5$ . It shows that the values of  $P^*$  and  $\eta^*$  for the irreversible single TBHE are higher than those of the combined TBHE. That is because there exist thermal resistances between the reservoir and the VM. The results about power output are consistent with the analyses of Refs. [107–109] for conventional macroscopic energy conversion systems, but the reasons

are different. The power of macro heat engine decreases due to the total thermal resistance increases, there are three reasons for the power reduction of the combined TBHE:

1. The irreversible combined TBHE is connected by intermediate reservoir, which leads to the increased overall heat resistance increase.
2. The TBHE exchange energy through particle moves, which is different from macro heat engine. The energy releasing from upper heat engine can't be absorbed completely by lower heat engine and as a result the efficiency decreases.
3. Because the intermediate reservoir is considered, the temperature of the reservoirs of upper heat engine changes and the velocity of particle motion changes. The upper heat engine absorbs less energy from the hot reservoir  $T_H$ . As a result, the total power output decreases.



(a)  $P^*$  characteristic of single and combined TBHE about  $U$ .



(b)  $\eta^*$  characteristic of single and combined TBHE about  $U$ .

Figure 13.  $P^*$  and  $\eta^*$  characteristics of single and combined TBHE about  $U$ .

Table 1. The power output performance comparisons between single and combined TBHE with  $U = 1.5$ .

External Load	$f=0$	$f=0.5$	$f=1$
Single TBHE $P^*$	0.768	0.812	0.857
Combined TBHE $P^*$	0.408	0.513	0.62
Increase of $P^*$	-46.9%	-36.8%	-27.7%

**Table 2.** The efficiency performance comparisons between single and combined TBHE with  $U = 1.5$ .

External Load	$f=0$	$f=0.5$	$f=1$
Single TBHE $\eta^*$	0.208	0.219	0.23
Combined TBHE $\eta^*$	0.122	0.154	0.186
Increase of $\eta^*$	−41.3%	−29.7%	−19.1%

It is supposed that the single or combined HE is operating between two heat reservoirs with fixed temperatures. For the one-stage TBHE, there are two heat transfer processes between two reservoirs. For the two-stage combined TBHE, the bottom HE has two heat transfer processes and there are four heat transfer processes in total. As a result, the overall heat resistance increases and the power and efficiency decrease. For the three-stage combined TBHE, two heat transfer processes are added, there are six heat transfer processes. As a result, the power and efficiency decrease continually. Therefore, as the number of HEs operating in tandem increases, the overall heat resistance increases and the power and efficiency decrease. Some scholars have studied the macro combined Carnot HE model and systematically expounded the effect of heat resistance on the performance of multi-stage combined Carnot HE [99,109].

One can find from the present analyses that, when the bottom TBHE is placed below the topping TBHE, the entire power output and efficiency can be greatly improved due to the expanded working temperature of the entire system. The results can be applied to the performance optimization of the combined energy conversion systems with multiple HRs.

## 7. Conclusions

In this paper, an irreversible combined thermal Brownian heat engine model is established by FTT theory. The effects of basic parameters on the performance of the combined thermal Brownian heat engine are analyzed with or without external load. The optimal thermodynamic performance of the combined thermal Brownian heat engine is further studied. The main conclusions are:

1. When the temperature ratio  $\tau$  is fixed, there is a specific optimal temperature ratio  $\omega$  which maximize power or efficiency. Reducing the heat leakage coefficient and enhancing the heat transfer between the thermal Brownian heat engines and reservoir can improve the performance. There are suitable barrier height and the ratio of barrier height to make the combined thermal Brownian heat engine work at optimum power and efficiency whether the potential field is affected by the external load or not.
2. When the potential field is free from external load, considering heat leakage and kinetic energy loss, the curves of  $P^* - \eta$  are loop-shaped ones and the optimal working regions are  $P_{\eta^*_{\max}}^* < P^* < P_{\max}^*$  and  $\eta_{P^*_{\max}}^* < \eta^* < \eta_{\max}^*$ . The maximum power and efficiency decrease first and then increase versus asymmetry of the potential.
3. When the potential field is influenced by external load, the steady current decreases with the increase of external load. The maximum power and efficiency monotonically increase versus the asymmetry of the potential. The power and efficiency are monotonically increasing versus external load.
4. The overall heat resistance of combined thermal Brownian heat engine is bigger than that of single thermal Brownian heat engine, the power or efficiency of combined thermal Brownian heat engine are lower than that of single thermal Brownian heat engine.

**Author Contributions:** Conceptualization, C.Q., Z.D. and L.C.; Data curation, Y.G. and H.F.; Funding acquisition, Z.D. and L.C.; Methodology, C.Q., Z.D., L.C. and H.F.; Software, C.Q., Z.D., Y.G. and H.F.; Supervision, L.C.; Validation, C.Q. and Z.D.; Writing—Original draft preparation, C.Q. and Z.D.; Writing—Reviewing and Editing, L.C. All authors have read and agreed to the published version of the manuscript.

**Funding:** This paper is supported by the National Natural Science Foundation of China (Project Nos. 51779262, 51576207 and 51306206), Hubei Provincial Natural Science Foundation of China (Project No. 2017CFB498) and the independent scientific research project of Naval University of Engineering (425317Q016).

**Acknowledgments:** The authors wish to thank the reviewers for their careful, unbiased and constructive suggestions, which led to this revised manuscript.

**Conflicts of Interest:** The authors declare no conflict of interest.

## Nomenclature

$A$	self-defined function
$a$	self-defined function
$B$	self-defined function
$b$	self-defined function
$C$	self-defined function
$C_i$	heat leakage coefficient ( $J/K$ )
$c$	self-defined function
$F$	external load
$f$	dimensionless external load
$G, H, I$	some defined functions
$J$	steady current
$k$	temperature ratio
$k_B$	Boltzmann constant ( $J/K$ )
$L$	length of potential field ( $m$ )
$n$	the ratio of barrier height
$P$	power output ( $W$ )
$Q$	heat flow rate ( $W$ )
$q_{kin}$	kinetic energy ( $W$ )
$q_L$	heat leakage rate ( $W$ )
$T$	temperature ( $K$ )
$U$	barrier height ( $J$ )
$v$	drift velocity of particle
$x, y$	self-defined functions
$z$	the position of particle
<b>Greek symbols</b>	
$\gamma$	friction coefficient
$\eta$	efficiency
$\mu$	asymmetry of the potential
$\omega, \tau$	temperature ratio
$\beta$	dimensionless heat leakage coefficient
<b>Abbreviations</b>	
CR	cold reservoir
FTT	Finite time thermodynamics
HE	heat engine
HR	hot reservoir
TBHE	thermal Brownian heat engine
VM	viscous medium

## References

1. Parrondo, J.M.R.; de Cisneros, B.J. Energetics of Brownian motors: A review. *Appl. Phys. A* **2002**, *75*, 179–191. [[CrossRef](#)]
2. Hänggi, P.; Marchesoni, F. Artificial Brownian motors: Controlling transport on the nanoscale. *Rev. Mod. Phys.* **2009**, *81*, 387–442. [[CrossRef](#)]
3. Mugnai, M.L.; Hyeon, C.; Hinczewski, M.; Thirumalai, D. Theoretical perspectives on biological machines. *Rev. Mod. Phys.* **2020**, *92*, 025001. [[CrossRef](#)]
4. Andresen, B.; Berry, R.S.; Ondrechen, M.J.; Salamon, P. Thermodynamics for processes in finite time. *Acc. Chem. Res.* **1984**, *17*, 266–271. [[CrossRef](#)]

5. Chen, L.G.; Wu, C.; Sun, F.R. Finite time thermodynamic optimization or entropy generation minimization of energy systems. *J. Non Equilib. Thermodyn.* **1999**, *24*, 327–359. [[CrossRef](#)]
6. Andresen, B. Current trends in finite-time thermodynamics. *Angew. Chem. Int. Ed.* **2011**, *50*, 2690–2704. [[CrossRef](#)]
7. Berry, R.S.; Salamon, P.; Andresen, B. How it all began. *Entropy* **2020**, *22*, 908. [[CrossRef](#)] [[PubMed](#)]
8. Hoffman, K.H.; Burzler, J.; Fischer, A.; Schaller, M.; Schubert, S. Optimal process paths for endoreversible systems. *J. Non Equilib. Thermodyn.* **2003**, *28*, 233–268. [[CrossRef](#)]
9. Zaeva, M.A.; Tsirlin, A.M.; Didina, O.V. Finite time thermodynamics: Realizability domain of heat to work converters. *J. Non Equilib. Thermodyn.* **2019**, *44*, 181–191. [[CrossRef](#)]
10. Masser, R.; Hoffmann, K.H. Endoreversible modeling of a hydraulic recuperation system. *Entropy* **2020**, *22*, 383. [[CrossRef](#)]
11. Kushner, A.; Lychagin, V.; Roop, M. Optimal thermodynamic processes for gases. *Entropy* **2020**, *22*, 448. [[CrossRef](#)] [[PubMed](#)]
12. De Vos, A. Endoreversible models for the thermodynamics of computing. *Entropy* **2020**, *22*, 660. [[CrossRef](#)]
13. Masser, R.; Khodja, A.; Scheunert, M.; Schwalbe, K.; Fischer, A.; Paul, R.; Hoffmann, K.H. Optimized piston motion for an alpha-type Stirling engine. *Entropy* **2020**, *22*, 700. [[CrossRef](#)] [[PubMed](#)]
14. Chen, L.G.; Ma, K.; Ge, Y.L.; Feng, H.J. Re-optimization of expansion work of a heated working fluid with generalized radiative heat transfer law. *Entropy* **2020**, *22*, 720. [[CrossRef](#)] [[PubMed](#)]
15. Tsirlin, A.; Gagarina, L. Finite-time thermodynamics in economics. *Entropy* **2020**, *22*, 891. [[CrossRef](#)]
16. Tsirlin, A.; Sukin, I. Averaged optimization and finite-time thermodynamics. *Entropy* **2020**, *22*, 912. [[CrossRef](#)] [[PubMed](#)]
17. Muschik, W.; Hoffmann, K.H. Modeling, simulation, and reconstruction of 2-reservoir heat-to-power processes in finite-time thermodynamics. *Entropy* **2020**, *22*, 997. [[CrossRef](#)]
18. Insinga, A.R. The quantum friction and optimal finite-time performance of the quantum Otto cycle. *Entropy* **2020**, *22*, 1060. [[CrossRef](#)]
19. Schön, J.C. Optimal control of hydrogen atom-like systems as thermodynamic engines in finite time. *Entropy* **2020**, *22*, 1066. [[CrossRef](#)]
20. Andresen, B.; Essex, C. Thermodynamics at very long time and space scales. *Entropy* **2020**, *22*, 1090. [[CrossRef](#)]
21. Chen, L.G.; Ma, K.; Feng, H.J.; Ge, Y.L. Optimal configuration of a gas expansion process in a piston-type cylinder with generalized convective heat transfer law. *Energies* **2020**, *13*, 3229. [[CrossRef](#)]
22. Scheunert, M.; Masser, R.; Khodja, A.; Paul, R.; Schwalbe, K.; Fischer, A.; Hoffmann, K.H. Power-optimized sinusoidal piston motion and its performance gain for an Alpha-type Stirling engine with limited regeneration. *Energies* **2020**, *13*, 4564. [[CrossRef](#)]
23. Boikov, S.Y.; Andresen, B.; Akhremenkov, A.A.; Tsirlin, A.M. Evaluation of irreversibility and optimal organization of an integrated multi-stream heat exchange system. *J. Non Equilib. Thermodyn.* **2020**, *45*, 155–171. [[CrossRef](#)]
24. Chen, L.G.; Feng, H.J.; Ge, Y.L. Maximum energy output chemical pump configuration with an infinite-low- and a finite-high-chemical potential mass reservoirs. *Energy Convers. Manag.* **2020**, *223*, 113261. [[CrossRef](#)]
25. Hoffmann, K.H.; Burzler, J.M.; Schubert, S. Endoreversible thermodynamics. *J. Non Equilib. Thermodyn.* **1997**, *22*, 311–355.
26. Wagner, K.; Hoffmann, K.H. Endoreversible modeling of a PEM fuel cell. *J. Non Equilib. Thermodyn.* **2015**, *40*, 283–294. [[CrossRef](#)]
27. Muschik, W. Concepts of phenomenological irreversible quantum thermodynamics I: Closed undecomposed Schottky systems in semi-classical description. *J. Non Equilib. Thermodyn.* **2019**, *44*, 1–13. [[CrossRef](#)]
28. Ponmurugan, M. Attainability of maximum work and the reversible efficiency of minimally nonlinear irreversible heat engines. *J. Non Equilib. Thermodyn.* **2019**, *44*, 143–153. [[CrossRef](#)]
29. Raman, R.; Kumar, N. Performance analysis of Diesel cycle under efficient power density condition with variable specific heat of working fluid. *J. Non Equilib. Thermodyn.* **2019**, *44*, 405–416. [[CrossRef](#)]
30. Schwalbe, K.; Hoffmann, K.H. Stochastic Novikov engine with Fourier heat transport. *J. Non Equilib. Thermodyn.* **2019**, *44*, 417–424. [[CrossRef](#)]
31. Morisaki, T.; Ikegami, Y. Maximum power of a multistage Rankine cycle in low-grade thermal energy conversion. *Appl. Therm. Eng.* **2014**, *69*, 78–85. [[CrossRef](#)]
32. Yasunaga, T.; Ikegami, Y. Application of finite time thermodynamics for evaluation method of heat engines. *Energy Procedia* **2017**, *129*, 995–1001. [[CrossRef](#)]
33. Yasunaga, T.; Fontaine, K.; Morisaki, T.; Ikegami, Y. Performance evaluation of heat exchangers for application to ocean thermal energy conversion system. *Ocean Therm. Energy Convers.* **2017**, *22*, 65–75.
34. Yasunaga, T.; Koyama, N.; Noguchi, T.; Morisaki, T.; Ikegami, Y. Thermodynamical optimum heat source mean velocity in heat exchangers on OTEC. In Proceedings of the Grand Renewable Energy 2018 Proceedings, Yokohama, Japan, 17–22 June 2018.
35. Yasunaga, T.; Noguchi, T.; Morisaki, T.; Ikegami, Y. Basic heat exchanger performance evaluation method on OTEC. *J. Mar. Sci. Eng.* **2018**, *6*, 32. [[CrossRef](#)]
36. Fontaine, K.; Yasunaga, T.; Ikegami, Y. OTEC maximum net power output using Carnot cycle and application to simplify heat exchanger selection. *Entropy* **2019**, *21*, 1143. [[CrossRef](#)]
37. Yasunaga, T.; Ikegami, Y. Finite-time thermodynamic model for evaluating heat engines in ocean thermal energy conversion. *Entropy* **2020**, *22*, 211. [[CrossRef](#)] [[PubMed](#)]
38. Yasunaga, T.; Ikegami, Y. Fundamental characteristics in power generation by heat engines on ocean thermal energy conversion (Construction of finite-time thermodynamic model and effect of heat source flow rate). *Trans. JSME* **2021**. in press (In Japanese) [[CrossRef](#)]

39. Feidt, M. Carnot cycle and heat engine: Fundamentals and applications. *Entropy* **2020**, *22*, 348. [[CrossRef](#)]
40. Feidt, M.; Costea, M. Effect of machine entropy production on the optimal performance of a refrigerator. *Entropy* **2020**, *22*, 913. [[CrossRef](#)]
41. Rogolino, P.; Cimmelli, V.A. Thermoelectric efficiency of Silicon–Germanium alloys in finite-time thermodynamics. *Entropy* **2020**, *22*, 1116. [[CrossRef](#)] [[PubMed](#)]
42. Essex, C.; Das, I. Radiative transfer and generalized wind. *Entropy* **2020**, *22*, 1153. [[CrossRef](#)]
43. Dann, R.; Kosloff, R.; Salamon, P. Quantum finite time thermodynamics: Insight from a single qubit engine. *Entropy* **2020**, *22*, 1255. [[CrossRef](#)] [[PubMed](#)]
44. Chen, L.G.; Feng, H.J.; Ge, Y.L. Power and efficiency optimization for open combined regenerative Brayton and inverse Brayton cycles with regeneration before the inverse cycle. *Entropy* **2020**, *22*, 677. [[CrossRef](#)]
45. Tang, C.Q.; Chen, L.G.; Feng, H.J.; Wang, W.H.; Ge, Y.L. Power optimization of a closed binary Brayton cycle with isothermal heating processes and coupled to variable-temperature reservoirs. *Energies* **2020**, *13*, 3212. [[CrossRef](#)]
46. Chen, L.G.; Shen, J.F.; Ge, Y.L.; Wu, Z.X.; Wang, W.H.; Zhu, F.L.; Feng, H.J. Power and efficiency optimization of open Maisotsenko–Brayton cycle and performance comparison with traditional open regenerated Brayton cycle. *Energy Convers. Manag.* **2020**, *217*, 113001. [[CrossRef](#)]
47. Chen, L.G.; Yang, B.; Feng, H.J.; Ge, Y.L.; Xia, S.J. Performance optimization of an open simple-cycle gas turbine combined cooling, heating and power plant driven by basic oxygen furnace gas in China’s steelmaking plants. *Energy* **2020**, *203*, 117791. [[CrossRef](#)]
48. Feng, H.J.; Chen, W.J.; Chen, L.G.; Tang, W. Power and efficiency optimizations of an irreversible regenerative organic Rankine cycle. *Energy Convers. Manag.* **2020**, *220*, 113079. [[CrossRef](#)]
49. Feng, H.J.; Wu, Z.X.; Chen, L.G.; Ge, Y.L. Constructal thermodynamic optimization for dual-pressure organic Rankine cycle in waste heat utilization system. *Energy Convers. Manag.* **2021**, *227*, 113585. [[CrossRef](#)]
50. Ge, Y.L.; Chen, L.G.; Feng, H.J. Ecological optimization of an irreversible Diesel cycle. *Eur. Phys. J. Plus* **2021**, *136*, 198. [[CrossRef](#)]
51. Tang, C.Q.; Chen, L.G.; Feng, H.J.; Ge, Y.L. Four-objective optimization for an irreversible closed modified simple Brayton cycle. *Entropy* **2021**, *23*, 282. [[CrossRef](#)] [[PubMed](#)]
52. Liu, X.W.; Chen, L.G.; Ge, Y.L.; Feng, H.J.; Wu, F.; Lorenzini, G. Exergy-based ecological optimization of an irreversible quantum Carnot heat pump with spin-1/2 systems. *J. Non Equilib. Thermodyn.* **2021**, *46*, 61–76. [[CrossRef](#)]
53. Wu, Z.X.; Feng, H.J.; Chen, L.G.; Tang, W.; Shi, J.Z.; Ge, Y.L. Constructal thermodynamic optimization for ocean thermal energy conversion system with dual-pressure organic Rankine cycle. *Energy Convers. Manag.* **2020**, *210*, 112727. [[CrossRef](#)]
54. Feng, H.J.; Qin, W.X.; Chen, L.G.; Cai, C.G.; Ge, Y.L.; Xia, S.J. Power output, thermal efficiency and exergy-based ecological performance optimizations of an irreversible KCS-34 coupled to variable temperature heat reservoirs. *Energy Convers. Manag.* **2020**, *205*, 112424. [[CrossRef](#)]
55. Qiu, S.S.; Ding, Z.M.; Chen, L.G. Performance evaluation and parametric optimum design of irreversible thermionic generators based on van der Waals heterostructures. *Energy Convers. Manag.* **2020**, *225*, 113360. [[CrossRef](#)]
56. Chen, L.G.; Meng, F.K.; Ge, Y.L.; Feng, H.J.; Xia, S.J. Performance optimization of a class of combined thermoelectric heating devices. *Sci. China Technol. Sci.* **2020**, *63*, 2640–2648. [[CrossRef](#)]
57. Chen, L.G.; Ge, Y.L.; Liu, C.; Feng, H.J.; Lorenzini, G. Performance of universal reciprocating heat-engine cycle with variable specific heats ratio of working fluid. *Entropy* **2020**, *22*, 397. [[CrossRef](#)] [[PubMed](#)]
58. Shi, S.S.; Ge, Y.L.; Chen, L.G.; Feng, H.J. Four-objective optimization of irreversible Atkinson cycle based on NSGA-II. *Entropy* **2020**, *22*, 1150. [[CrossRef](#)]
59. Wu, H.; Ge, Y.L.; Chen, L.G.; Feng, H.J. Power, efficiency, ecological function and ecological coefficient of performance optimizations of an irreversible Diesel cycle based on finite piston speed. *Energy* **2021**, *216*, 119235. [[CrossRef](#)]
60. Ahmadi, M.H.; Pourkiaei, S.M.; Ghazvini, M.; Pourfayaz, F. Thermodynamic assessment and optimization of performance of irreversible Atkinson cycle. *Iran. J. Chem. Chem. Eng.* **2020**, *39*, 267–280.
61. Ahmadi, M.H.; Mohammadi, A.H.; Dehghani, S.; Barranco-Jimenez, M.A. Multi-objective thermodynamic-based optimization of output power of Solar Dish–Stirling engine by implementing an evolutionary algorithm. *Energy Convers. Manag.* **2013**, *75*, 438–445. [[CrossRef](#)]
62. Ahmadi, M.H.; Ahmadi, M.A.; Mohammadi, A.H.; Feidt, M.; Pourkiaei, S.M. Multi-objective optimization of an irreversible Stirling cryogenic refrigerator cycle. *Energy Convers. Manag.* **2014**, *82*, 351–360. [[CrossRef](#)]
63. Ahmadi, M.H.; Jokar, M.A.; Ming, T.Z.; Feidt, M.; Pourfayaz, F.; Astaraei, F.R. Multi-objective performance optimization of irreversible molten carbonate fuel cell–Braysson heat engine and thermodynamic analysis with ecological objective approach. *Energy* **2018**, *144*, 707–722. [[CrossRef](#)]
64. Jokar, M.A.; Ahmadi, M.H.; Sharifpur, M.; Meyer, J.P.; Pourfayaz, F.; Ming, T.Z. Thermodynamic evaluation and multi-objective optimization of molten carbonate fuel cell–supercritical CO<sub>2</sub> Brayton cycle hybrid system. *Energy Convers. Manag.* **2017**, *153*, 538–556. [[CrossRef](#)]
65. Ghasemkhani, A.; Farahat, S.; Naserian, M.M. Multi-objective optimization and decision making of endoreversible combined cycles with consideration of different heat exchangers by finite time thermodynamics. *Energy Convers. Manag.* **2018**, *171*, 1052–1062. [[CrossRef](#)]

66. Chen, L.G.; Tang, C.Q.; Feng, H.J.; Ge, Y.L. Power, efficiency, power density and ecological function optimizations for an irreversible modified closed variable-temperature reservoir regenerative Brayton cycle with one isothermal heating process. *Energies* **2020**, *13*, 5133. [[CrossRef](#)]
67. Zhang, L.; Chen, L.G.; Xia, S.J.; Ge, Y.L.; Wang, C.; Feng, H.J. Multi-objective optimization for helium-heated reverse water gas shift reactor by using NSGA-II. *Int. J. Heat Mass Transf.* **2020**, *148*, 119025. [[CrossRef](#)]
68. Sun, M.; Xia, S.J.; Chen, L.G.; Wang, C.; Tang, C.Q. Minimum entropy generation rate and maximum yield optimization of sulfuric acid decomposition process using NSGA-II. *Entropy* **2020**, *22*, 1065. [[CrossRef](#)]
69. Asfaw, M.; Bekele, M. Current, maximum power and optimized efficiency of a Brownian heat engine. *Eur. Phys. J. B* **2004**, *38*, 457–461. [[CrossRef](#)]
70. Asfaw, M.; Bekele, M. Energetics of a simple microscopic heat engine. *Phys. Rev. E* **2005**, *72*, 056109. [[CrossRef](#)] [[PubMed](#)]
71. Asfaw, M.; Bekele, M. Exploring the operation of a tiny heat engine. *Phys. A* **2007**, *384*, 346–358. [[CrossRef](#)]
72. Van den Broeck, C.; Kawai, R. Brownian refrigerator. *Phys. Rev. Lett.* **2006**, *96*, 210601. [[CrossRef](#)]
73. Ding, Z.M.; Chen, L.G.; Sun, F.R. Generalized model and optimum performance of an irreversible thermal Brownian microscopic heat pump. *Math. Comput. Model.* **2011**, *53*, 780–792. [[CrossRef](#)]
74. Van den Broek, M.; Van den Broeck, C. Chiral Brownian heat pump. *Phys. Rev. Lett.* **2008**, *100*, 130601. [[CrossRef](#)]
75. Zhang, Y.P.; He, J.Z. Thermodynamic performance characteristics of an irreversible micro-Brownian heat engine driven by temperature difference. *Chin. Phys. Lett.* **2010**, *27*, 090502.
76. Zhang, Y.; Lin, B.H.; Chen, J.C. Performance characteristics of an irreversible thermally driven Brownian microscopic heat engine. *Eur. Phys. J. B* **2006**, *53*, 481–485. [[CrossRef](#)]
77. Ai, B.Q.; Xie, H.Z.; Wen, D.H.; Liu, L.G. Heat flow and efficiency in a microscopic engine. *Eur. Phys. J. B* **2005**, *48*, 101–106. [[CrossRef](#)]
78. Ai, B.Q.; Wang, L.; Liu, L.G. Brownian micro-engines and refrigerators in a spatially periodic temperature field: Heat flow and performances. *Phys. Lett. A* **2006**, *352*, 286–290. [[CrossRef](#)]
79. Asfaw, M. Effect of thermal inhomogeneity on the performance of a Brownian heat engine. *Eur. Phys. J. B* **2013**, *86*, 189. [[CrossRef](#)]
80. Gao, T.F.; Zhang, Y.; Chen, J.C. The Onsager reciprocity relation and generalized efficiency of a thermal Brownian motor. *Chin. Phys. B* **2009**, *18*, 3279–3286.
81. Asfaw, M. Modeling an efficient Brownian heat engine. *Eur. Phys. J. B* **2008**, *65*, 109–116. [[CrossRef](#)]
82. Gao, T.F.; Chen, J.C. Non-equilibrium thermodynamic analysis on the performance of an irreversible thermally driven Brownian motor. *Mod. Phys. Lett. B* **2010**, *24*, 325–333. [[CrossRef](#)]
83. Machura, L.; Kostur, M.; Talkner, P.; Luczka, J.; Marchesoni, F.; Hanggi, P. Brownian motors: Current fluctuations and rectification efficiency. *Phys. Rev. E* **2004**, *70*, 061105. [[CrossRef](#)] [[PubMed](#)]
84. Van den Broeck, C.; Kawai, R.; Meurs, P. Microscopic analysis of a thermal Brownian motor. *Phys. Rev. Lett.* **2004**, *93*, 090601. [[CrossRef](#)] [[PubMed](#)]
85. Feito, M.; Cao, F.J. Information and maximum power in a feedback controlled Brownian ratchet. *Euro. Phys. J. B* **2007**, *59*, 63–68. [[CrossRef](#)]
86. Qian, M.; Zhang, X.; Wilson, R.J.; Feng, J. Efficiency of Brownian motors in terms of entropy production rate. *EPL* **2008**, *84*, 10014. [[CrossRef](#)]
87. Schönborn, J.B.; Herges, R.; Hartke, B. Brownian molecular rotors: Theoretical design principles and predicted realizations. *J. Chem. Phys.* **2009**, *130*, 234906. [[CrossRef](#)] [[PubMed](#)]
88. Santillan, M.; Mackey, M.C. Dynamic stability versus thermodynamic performance in a simple model for a Brownian motor. *Phys. Rev. E* **2008**, *78*, 061122. [[CrossRef](#)] [[PubMed](#)]
89. Luo, X.G.; Liu, N.; He, J.Z. Optimum analysis of a Brownian refrigerator. *Phys. Rev. E* **2013**, *87*, 022139. [[CrossRef](#)]
90. Rozenbaum, V.M.; Makhnovskii, Y.A.; Shapochkina, I.V.; Sheu, S.Y.; Yang, D.Y.; Lin, S.H. Adiabatically driven Brownian pumps. *Phys. Rev. E* **2013**, *87*, 012104. [[CrossRef](#)]
91. Asfaw, M. Thermodynamic feature of a Brownian heat engine operating between two heat baths. *Phys. Rev. E* **2014**, *89*, 012143. [[CrossRef](#)]
92. Spiechowicz, J.; Hänggi, P.; Łuczka, J. Brownian motors in the microscale domain: Enhancement of efficiency by noise. *Phys. Rev. E* **2014**, *90*, 032104. [[CrossRef](#)]
93. Taye, M.A. Exact analytical thermodynamic expressions for a Brownian heat engine. *Phys. Rev. E* **2015**, *92*, 032126. [[CrossRef](#)]
94. Dinis, L.; Martínez, I.A.; Roldán, É.; Parrondo, J.M.R.; Rica, R.A. Thermodynamics at the microscale: From effective heating to the Brownian Carnot engine. *J. Stat. Mech. Theor. Exp.* **2016**, *19*, 054003. [[CrossRef](#)]
95. Martínez, I.A.; Roldán, E.; Dinis, L.; Petrov, D.; Parrondo, J.M.R.; Rica, R.A. Brownian Carnot engine. *Nat. Phys.* **2016**, *12*, 67–70. [[CrossRef](#)]
96. Park, J.M.; Chun, H.M.; Noh, J.D. Efficiency at maximum power and efficiency fluctuations in a linear Brownian heat-engine model. *Phys. Rev. E* **2016**, *94*, 012127.
97. Açıkkaalp, E. Analysis of a Brownian heat engine with ecological criteria. *Eur. Phys. J. Plus* **2016**, *131*, 426. [[CrossRef](#)]
98. Tutu, H.; Ouchi, K.; Horita, T. Performance optimization in two-dimensional Brownian rotary ratchet models. *Phys. Rev. E* **2017**, *95*, 062103. [[CrossRef](#)]
99. Nicolis, G.; De Decker, Y. Stochastic thermodynamics of Brownian motion. *Entropy* **2017**, *19*, 434. [[CrossRef](#)]

100. Defaveri, L.A.; Morgado, W.A.; Queirós, S.M. Power output for a nonlinear Brownian machine. *Phys. Rev. E* **2017**, *96*, 052115. [[CrossRef](#)]
101. Kanada, R.; Shinagawa, R.; Sasaki, K. Diffusion enhancement of Brownian motors revealed by a solvable model. *Phys. Rev. E* **2018**, *98*, 062110. [[CrossRef](#)]
102. Herpich, T.; Shayanfar, K.; Esposito, M. Effective thermodynamics of two interacting underdamped Brownian particles. *Phys. Rev. E* **2020**, *101*, 022116. [[CrossRef](#)]
103. Lee, J.S.; Park, J.M.; Park, H. Brownian heat engine with active reservoirs. *Phys. Rev. E* **2020**, *102*, 032116. [[CrossRef](#)]
104. Holubec, V.; Steffenoni, S.; Falasco, G.; Kroy, K. Active Brownian heat engines. *Phys. Rev. Res.* **2020**, *2*, 043262. [[CrossRef](#)]
105. Holubec, V.; Marathe, R. Underdamped active Brownian heat engine. *Phys. Rev. E* **2020**, *102*, 060101(R). [[CrossRef](#)] [[PubMed](#)]
106. Chimal-Eguia, J.C.; Paez-Hernández, R.T.; Pacheco-Paez, J.C. Comparative performance analysis of a Brownian Carnot cycle from the perspective of a stochastic model against the linear irreversible thermodynamics theory. *Phys. A Stat. Mech. Appl.* **2021**, *570*, 125743. [[CrossRef](#)]
107. Rubin, M.H.; Andresen, B. Optimal staging of endoreversible heat engines. *J. Appl. Phys.* **1982**, *53*, 1–7. [[CrossRef](#)]
108. Wu, C. Power performance of a cascade endoreversible cycle. *Energy Convers. Manag.* **1990**, *30*, 261–266. [[CrossRef](#)]
109. Chen, J.C. A universal model of an irreversible combined Carnot cycle system and its general performance characteristics. *J. Phys. A Math. Gen.* **1998**, *31*, 3383–3394. [[CrossRef](#)]
110. Ozkaynak, S. The theoretical efficiency limits for a combined cycle under the condition of maximum power output. *J. Phys. D Appl. Phys.* **1995**, *28*, 2024–2028. [[CrossRef](#)]
111. Sahin, B.; Kodal, A. Steady-state thermodynamic analysis of a combined Carnot cycle with internal irreversibility. *Energy* **1995**, *20*, 1285–1289. [[CrossRef](#)]
112. De Vos, A.; Chen, J.C.; Andresen, B. Analysis of combined systems of two endoreversible engines. *Open Syst. Inf. Dyn.* **1997**, *4*, 3–13. [[CrossRef](#)]
113. El Haj Assad, M. Finite-time thermodynamic analysis of combined heat engines. *Int. J. Mech. Eng. Educ.* **1997**, *25*, 281–289. [[CrossRef](#)]
114. Lewins, J.D. Optimizing cascades of endo-reversible heat engines. *Int. J. Mech. Eng. Educ.* **1999**, *27*, 91–101. [[CrossRef](#)]
115. Cheng, X.T.; Liang, X.G. Optimization of combined endoreversible Carnot heat engines with different objectives. *Chin. Phys. B* **2015**, *24*, 60510. [[CrossRef](#)]
116. Wu, J. A new approach to determining the intermediate temperatures of endoreversible combined cycle power plant corresponding to maximum power. *Int. J. Heat Mass Transf.* **2015**, *91*, 150–161. [[CrossRef](#)]
117. Iyyappan, I.; Johal, R.S. Efficiency of a two-stage heat engine at optimal power. *EPL* **2019**, *128*, 50004. [[CrossRef](#)]
118. Levario-Medina, S.; Valencia-Ortega, G.; Barranco-Jimenez, M.A. Energetic optimization considering a generalization of the ecological criterion in traditional simple-cycle and combined cycle power plants. *J. Non Equilib. Thermodyn.* **2020**, *45*, 269–290. [[CrossRef](#)]
119. Meng, Z.W.; Chen, L.G.; Wu, F. Optimal power and efficiency of multi-stage endoreversible quantum carnot heat engine with Harmonic oscillators at the classical limit. *Entropy* **2020**, *22*, 457. [[CrossRef](#)]
120. Chen, L.G.; Meng, Z.W.; Ge, Y.L.; Wu, F. Performance analysis and optimization for irreversible combined Carnot heat engine working with ideal quantum gases. *Entropy* **2021**, in press.
121. Cheng, H.T.; He, J.Z.; Xiao, Y.L. Brownian heat engine driven by temperature difference in a periodic double-barrier sawtooth potential. *Acta Phys. Sin.* **2012**, *61*, 010502. (In Chinese)
122. Zhang, Y.P.; He, J.Z.; He, X.; Xiao, Y.L. Thermodynamic performance characteristics of a Brownian microscopic heat engine driven by discrete and periodic temperature field. *Commun. Theor. Phys.* **2010**, *54*, 857–862. [[CrossRef](#)]
123. Lin, B.H.; Chen, J.C. Performance characteristics and parametric optimum criteria of a Brownian micro-refrigerator in a spatially periodic temperature field. *J. Phys. A Math. Theor.* **2009**, *42*, 075006. [[CrossRef](#)]
124. Bejan, A. *Entropy Generation through Heat and Fluid Flow*; Wiley: New York, NY, USA, 1982.
125. Bejan, A. Theory of heat transfer-irreversible power plant. *Int. J. Heat Mass Transf.* **1988**, *31*, 1211–1219. [[CrossRef](#)]
126. Bejan, A. Theory of heat transfer-irreversible power plants. II. The optimal allocation of heat exchange equipment. *Int. J. Heat Mass Transf.* **1995**, *38*, 433–444. [[CrossRef](#)]